

Spin Squeezing in Electron Microscopy

Shiran Even-Haim^{*1}, Ethan Nussinson^{*1}, Roni Ben-Maimon², Alexey Gorlach¹, Ron Ruimy¹, Ephraim Shahmoon², Osip Schwartz^{†3}, Ido Kaminer^{†1}

¹*Faculty of Electrical & Computer Engineering and Solid-State Institute, Technion - Israel Institute of Technology, Haifa 3200003, Israel*

²*Department of Chemical & Biological Physics, Weizmann Institute of Science, Rehovot 7610001, Israel*

³*Department of Physics of Complex Systems, Weizmann Institute of Science, Rehovot 7610001, Israel*

^{*}[†]*equal contributors*

[†]kaminer@technion.ac.il [†]osip@weizmann.ac.il

Quantum metrology experiments in atomic physics and quantum optics have demonstrated measurement accuracy beyond the shot-noise limit via multi-particle entanglement. At the same time, electron microscopy—an essential tool for high-resolution imaging of biological systems—is severely constrained in its signal-to-noise ratio (SNR) by shot noise, due to the dose limit imposed by electron beam-induced damage. Here, we show theoretically that spin squeezing, a form of quantum metrology based on entanglement, is a natural fit for improving the SNR in electron microscopy. We investigate the generation of the necessary entangled states through electron-electron Coulomb interactions and quantum non-demolition measurements. Our results connect the fields of quantum metrology and electron interferometry, paving the way toward electron microscopy with SNR beyond the shot-noise limit.

1. Introduction

Transmission electron microscopes (TEM) leverage the short de Broglie wavelength of electrons to achieve atomic resolution. However, electron beam-induced damage significantly restricts the TEM’s ability to image many soft-matter samples, including most samples of interest in life sciences. For example, biological samples imaged in high-resolution cryogenic electron microscopy (cryo-EM) are constrained to an electron dose of around 20 electrons per square Angstrom[1] by radiation damage.

Cryo-EM has achieved extraordinary success in determining the structure of biological macromolecules with atomic resolution, overcoming the limited signal-to-noise ratio (SNR) by combining TEM image data from thousands or even millions of identical macromolecules or molecular complexes [2]. However, this approach cannot be applied to samples with unique,

non-repeating structures, such as lamellae (slices) ion-milled from whole cells, often studied with cryogenic electron tomography (cryo-ET). As life science studies using electron microscopy increasingly focus on such samples, improving their SNR becomes a key challenge.

In cryo-EM, images are generated by detecting the position-dependent phase ϕ imprinted by the sample on the electron's wave function. Under ideal conditions, the phase measurement accuracy is limited by shot noise, resulting in a phase uncertainty of $\Delta\phi_{\text{SQL}} = N^{-1/2}$, where N is the number of electrons per pixel, representing a fundamental constraint known as the standard quantum limit (SQL).

More specifically, information about the sample structure is contained in the small location-to-location variations of the phase, whereas the mean phase shift $\langle\phi\rangle$, determined by the sample's average thickness and composition, plays no role in imaging: inline interferometry conventionally used in cryo-EM is not sensitive to $\langle\phi\rangle$, and in off-axis interferometry schemes, it can generally be balanced out by adjusting the reference arm length. Throughout this paper, we therefore assume without loss of generality that $\langle\phi\rangle = 0$, and $\phi \ll 1$. Furthermore, since $\langle\phi\rangle$ can be measured with a negligible per-pixel electron dose, this assumption does not affect the SQL-limited uncertainty of the phase.

In practice, cryo-EM operates close to the SQL. Direct electron detectors [3,4] enable shot-noise-limited counting of electrons passing through each pixel. The phase profile is conventionally converted to amplitude variation by defocusing the TEM's imaging system, which results in a contrast transfer function that oscillates with spatial frequency, achieving near-SQL SNR at the maxima of the oscillations. Recently developed Zernike-like phase plates for TEM [5,6] enable efficient conversion of the phase profile to amplitude modulation without defocusing, approaching the SQL with a more uniform contrast transfer function. Further progress in cryo-EM and cryo-ET calls for new methods with phase accuracy surpassing the SQL.

Quantum physics can be harnessed to improve the SNR beyond the SQL, with the ultimate bound set by the Heisenberg limit [7], corresponding to a phase uncertainty of $\Delta\phi_{\text{H}} = N^{-1}$. Several quantum metrology approaches have been proposed for achieving sub-shot-noise-limited SNR in electron microscopy [8–10]. These can be broadly grouped into two classes. One consists of single-electron signal enhancement approaches, such as multi-pass

microscopy [11,12] or interaction-free measurements [8,13]. The other is based on multi-electron entangled states, such as electron NOON (or GHZ) states [14–16]. A pioneering effort in this direction explores using superconducting quantum circuits coupled to a TEM [17,18]. None of these approaches have yet achieved an experimental demonstration of quantum-enhanced electron interferometry.

At the same time, in other fields, quantum metrology has achieved measurement accuracy well beyond the shot noise limit. A central concept within the field of quantum metrology is quantum *squeezing*, the reduction of the quantum fluctuations of an observable to improve the measurement accuracy. Metrological improvements via squeezing were demonstrated in, e.g., light interferometry [19–21], nonlinear microscopy [22–24], or dark matter searches [25]. A particular type of squeezing, known as *spin squeezing* [26], applicable to quantum systems characterized by a collective spin or pseudo-spin, plays a central role in quantum metrology experiments with atomic ensembles [27–35].

In this work, we introduce the concept of *spin squeezing* to electron microscopy and show that it enables a significant improvement of phase measurement accuracy under realistic parameters. We envision an electron microscope implemented as a scanning interferometer [36,37] that creates images pixel by pixel, measuring the sample-induced phase shift in each point (Fig. 1a, b). Each electron passing through the interferometer is in a quantum superposition of being either in one arm of the interferometer or in the other. We use the two possible paths as the basis states, analogous to the two states of spin- $\frac{1}{2}$ particles, to define a pseudo-spin degree of freedom for each electron [26]. We then explore practical means to generate multi-electron quantum states that are spin-squeezed with respect to this “which-path” degree of freedom and show that such states enable a substantial reduction of shot noise-induced phase uncertainty under conditions relevant to cryo-EM. Spin squeezing of free electrons thus offers a natural avenue toward quantum-enhanced electron microscopy with SNR well above the SQL.

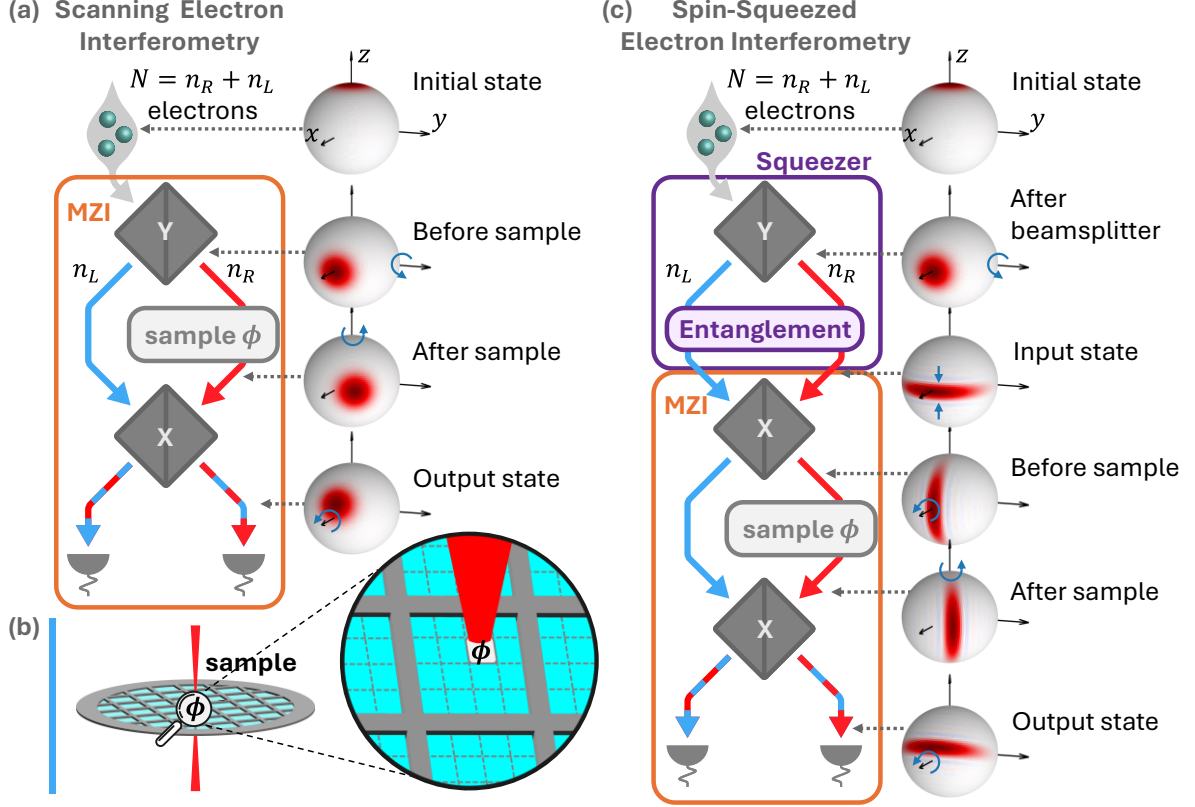


Fig. 1: Squeezing in electron interferometry. (a) Scanning electron Mach-Zehnder interferometer (MZI): multi-electron states are shown on the Bloch sphere, representing Wigner functions at different stages. An incoming N -electron state is rotated by $\pi/2$ about the y -axis by the first beamsplitter, initializing a superposition between the two arms. The electrons in the right arm interact with the sample, acquiring a phase ϕ , corresponding to ϕ -rotation around the z -axis. Finally, a second beamsplitter induces $\pi/2$ rotation about the x -axis, and a measurement of the number of electrons in each port is performed (measuring the z projection of the collective spin). (b) The sample is scanned (red beam) pixel by pixel. (c) Spin-squeezed electron interferometry: we introduce a preparation stage, referred to as the squeezer, where a multi-electron spin-squeezed state is prepared before being coupled into the MZI. The first beamsplitter of the MZI aligns the squeezed axis with the direction of the phase ϕ accumulation, thus enhancing the precision of the phase measurement.

This paper is organized as follows. In Section 2, we define the concept of spin squeezing in the context of electron interferometry. Then, in Section 3, we outline two different approaches for building an electron ‘squeezer’ device that prepares a batch of electrons in a spin-squeezed state (Fig. 1c). The first, described in Section 3.1, is an interaction-based method, where electron-electron interactions create entanglement between the states of individual electrons, generating spin squeezing. The second approach, described in Section 3.2, is a measurement-based method, where the electron interaction with a measuring device implements a quantum non-demolition measurement, entangling the electron states and inducing spin squeezing. In both cases, we determine the upper bound of the achievable phase

measurement accuracy based on quantum Fisher information and evaluate the phase accuracy attainable in a conventional interferometric measurement with such squeezed states. Furthermore, we outline potential experimental implementations for each method. We then turn to discussion and outlook in Section 4.

2. Interferometry with spin-squeezed electron states

A Mach-Zehnder interferometer (Fig. 1a) measures the relative phase between two paths—one that interacts with the sample and the other that serves as a reference. We consider a scenario where a batch of electrons is used to measure the phase at each pixel of the sample. For each electron, we denote the electron states passing through the right and left arms of the interferometer as $|R\rangle_n$ and $|L\rangle_n$, respectively, where $n \in \{1, \dots, N\}$ denotes the index of an electron within the batch of N electrons. In this notation, each electron is assigned a pseudo-spin operator described by the spin- $1/2$ Pauli operators σ_n^i with $i \in \{x, y, z\}$. The states $|L\rangle_n$ and $|R\rangle_n$ correspond to the north and south poles of the Bloch sphere representation of the spin, respectively, and satisfy $\hat{\sigma}_n^z |L\rangle_n = |L\rangle_n$, $\hat{\sigma}_n^z |R\rangle_n = -|R\rangle_n$. A phase shift between the interferometer arms (e.g., due to interaction with a sample) corresponds to a rotation around the z -axis. A beamsplitter couples the two paths, performing rotations around the x or y axis, with the rotation angle set by the magnitude of its coupling coefficient.

2.1 Electrons as quasi-distinguishable particles

An important consideration in electron microscopy is that the electron density is low enough such that the wave functions of different electrons in the beam do not overlap. As a result, the Pauli exclusion principle does not prohibit multiple electrons in the beam from traveling through the same arm of the interferometer. Thus, even though electrons are fundamentally indistinguishable particles, they can be treated as distinguishable under these conditions, allowing us to attribute individual spin operators $\hat{\sigma}_i^n$ to each electron.

Furthermore, we assume that each electron's pseudospin wave function undergoes the same sequence of transformations in the interferometer. Under these conditions, the multi-electron wave function remains symmetric with respect to the exchange of pseudospins, and therefore an ensemble of N electrons can be described as a single system with a spin $N/2$ [38,26]. The collective spin operators are given by $\hat{S}_i = \frac{1}{2} \sum_{n=1}^N \hat{\sigma}_i^n$. We define number

operators in the left and right paths, \hat{n}_L and \hat{n}_R , where $\hat{n}_R = \frac{N}{2} - \hat{S}_z$, such that the total number of electrons is conserved: $\hat{n}_L + \hat{n}_R = N$. The symmetric multi-electron state with n_R electrons in the right path is denoted as $|n_L, n_R\rangle = |N - n_R, n_R\rangle$. These collective spin states are also known as Dicke states.

The interferometer operation is composed of a sequence of steps (Fig. 1a), each described as a rotation of the collective spin. In a conventional interferometer, with uncorrelated electrons, the input state is created by the first beamsplitter that applies a y -axis rotation operator $e^{\frac{i\pi}{2}\hat{S}_y}$ on the initial state $|N, 0\rangle$. This operator produces the same state in each electron $\frac{1}{\sqrt{2}}(|L\rangle_n + |R\rangle_n)$, creating the coherent spin state $|\psi_0\rangle = \prod_{n=1}^N (|L\rangle_n + |R\rangle_n)$. The electrons then accumulate a relative phase between the two paths due to their interaction with the sample (Fig. 1b), represented by the operator $e^{i\phi\hat{S}_z}$, corresponding to a rotation around the z -axis by an angle ϕ . A second beamsplitter then applies a x -axis rotation $e^{\frac{i\pi}{2}\hat{S}_x}$.

Finally, the spin projection along the z -axis is measured by detecting the difference in the number of electrons arriving in the two output ports of the interferometer: $S_z = \frac{n_L - n_R}{2N}$. The phase ϕ is then determined using the relation:

$$S_z = \frac{N}{2} \sin \phi. \quad (1)$$

Interferometry with spin-squeezed electron states can be similarly described, by applying a similar interferometer sequence to a squeezed initial state, as illustrated in Fig. 1c.

The collective spin state at every stage can be visualized using the Wigner function [39] defined on the Bloch sphere, shown in Fig. 1a, c. All the expectation values and uncertainties of collective spin operators \hat{S}_i can be calculated as expectation values using the Wigner function as a probability distribution of the collective spin variables (S_x, S_y, S_z) .

2.2 Quantifying spin squeezing

The accuracy of the interferometric phase measurements described above, with the phase determined according to Eq. (1), is limited by quantum projection noise. The root-mean-square phase uncertainty $\Delta\phi_W$ can be calculated in terms of the spin operators [40]:

$$\Delta\phi_W = \frac{\sqrt{\langle(\hat{S}_y - \langle\hat{S}_y\rangle)^2\rangle}}{|\langle\hat{S}_x\rangle|}. \quad (2)$$

The spin components here refer to the section of the MZI before the interaction with the sample, where the uncertainty ellipse is squeezed along the y axis and expanded in the z axis (Fig. 3c).

For a coherent spin state, the phase uncertainty of Eq. (2) follows the SQL, $\Delta\phi_W = \Delta\phi_{\text{SQL}} = N^{-1/2}$. For a general spin state, the phase uncertainty can be quantified by Wineland's spin-squeezing parameter ξ^2 [40–42], defined as $\xi^2 = (\Delta\phi_W)^2 / (\Delta\phi_{\text{SQL}})^2$. A spin-squeezed state is characterized by $\xi^2 < 1$, indicating that the phase uncertainty is reduced below the SQL.

An alternative measure of phase estimation accuracy is the quantum Fisher information F [43,16], which quantifies the minimal possible phase measurement uncertainty for a given quantum state of electrons in the interferometer. For a pure state, the quantum Fisher information is given by $F = 4 \langle(\hat{S}_z - \langle\hat{S}_z\rangle)^2\rangle$, and the related phase sensitivity is:

$$\Delta\phi_F = F^{-1/2} = \frac{1}{2\sqrt{\langle(\hat{S}_z - \langle\hat{S}_z\rangle)^2\rangle}}. \quad (3)$$

In a conventional interferometer limited by the SQL, $F = N$, and in the Heisenberg limit, $F = N^2$. For a squeezed state, the increased uncertainty of \hat{S}_z corresponds to increased Fisher information and reduced phase uncertainty $\Delta\phi_F$.

Both the spin squeezing parameter ξ^2 and the quantum Fisher information F are useful for quantifying the phase estimation accuracy. The quantum Fisher information-derived phase uncertainty $\Delta\phi_F$ provides the theoretical lower bound of the phase uncertainty (the quantum Cramér Rao bound [44]), although a measurement protocol that can achieve this limit is only known in certain specific cases. In contrast, $\Delta\phi_W$ indicates the phase uncertainty achievable using conventional interferometric protocols where the phase is determined according to Eq. (1). Notably, the two uncertainties coincide for a coherent spin state, retrieving $\Delta\phi_{\text{SQL}}$.

3. Implementations

We propose two methods for achieving electron spin squeezing. The first is interaction-based squeezing, which results in one-axis twisting. The second is measurement-based

squeezing, which utilizes quantum non-demolition measurements. Both methods can potentially reach quantum Fisher information approaching the Heisenberg scaling. We further show that both methods can generate squeezed states ($\xi^2 < 1$) and therefore offer a practical path toward improving phase sensitivity beyond the shot-noise limit.

3.1 Interaction-based squeezer

The proposed interaction-based squeezer utilizes the Coulomb repulsion between electrons to generate squeezing. Coulomb interactions at the electron densities typical for cryo-EM are not strong enough to significantly affect the electron’s trajectories. However, these interactions can induce a significant phase shift in the electrons’ wave functions. For instance, two electrons separated by 2.6 cm – a typical distance at an electron energy of 100 keV and a beam current of 1 nA (readily achievable with a field-emission electron gun) – experience an interaction-induced phase shift of approximately 0.51 radians after propagating for 1 meter.

In conventional phase-contrast TEM imaging, these phase shifts are not observable because the distances between electrons typically far exceed the electron beam diameter and the length of electron wave packets. As a result, the Coulomb interaction shifts the phase of the entire wave packet uniformly, leading to no observable change in TEM images. However, the Coulomb phase can become significant in a Mach-Zehnder interferometer where the arms are separated by a distance comparable to or greater than the average interval between electrons.

A significant challenge in taking advantage of the electrons’ Coulomb interaction for spin squeezing is the stochastic distribution of distances between electrons, leading to a significant phase noise. This could be mitigated by designing an interferometer with electrons in the two arms propagating in opposite directions [15]. However, generating electrons in a coherent superposition of high-energy counter-propagating wave packets poses a separate, and still unsolved, challenge.

We propose a solution to the phase noise problem by replacing the pairwise, distance-dependent Coulomb interaction with a distance-independent, collective interaction. We envision passing the two arms of the interferometer through conductive channels (Fig. 2a). The channel length l is assumed to be large enough for all N electrons to be inside the channel simultaneously. The channel radius r is designed to be much smaller than the distance between

electrons in the same channel. The channels are also assumed to be either at low enough temperature or superconductive, so that the thermally induced dephasing [45] can be neglected.

In this setup, the Coulomb interaction will cause a phase shift in the interferometer that depends on the number of electrons in each arm. Specifically, the pair of conducting channels functions as a capacitor with mutual capacitance C , where the imbalance in electron numbers between the left and right arms induces an electric potential difference $V = e(n_R - n_L)/(2C)$. This potential induces an interferometric phase shift in each electron, resulting in a collective electron-electron interaction. At the same time, the pairwise distance-dependent Coulomb interactions of electrons in the same channel are suppressed by the screening effect (SM Section 1.1) of the narrow conducting channels. Thus, passing the interferometer arms through the pair of conductive, capacitively coupled channels replaces the pairwise Coulomb interactions between electrons with a phase shift that depends only on the electron count in each arm. Here, we focus on the non-relativistic approximation, leaving a rigorous relativistic analysis to future work.

The dependence of each electron's phase on the distribution of other electrons between the two channels creates quantum entanglement between the electrons. This entanglement can be described by including in the system Hamiltonian the total electrostatic energy of the capacitor $U = \frac{e^2(n_R - n_L)^2}{8C}$ (SM Section 1.1). Thus, the transformation performed by the two-channel device on the input electron state can be described by the operator:

$$S_{\text{int}} = e^{-\frac{i\chi_{\text{int}}S_z^2}{2}}. \quad (4)$$

with the interaction strength parameter $\chi_{\text{int}} = \frac{e^2 l}{v\hbar c}$, with l being the channel length and v the electrons' velocity. The transformation produced by this operator is known as one-axis twisting, and it generates a spin squeezed state that can be used for sub-shot-noise metrology as illustrated in Fig. 2.

For example, for cylindrical channels, shown in Fig. 2a., the mutual capacitance can be approximated as $C = \frac{l\epsilon_0\pi}{\text{arccosh}(\frac{d}{2r})}$ [46]. In this case, the interaction strength takes the form $\chi_{\text{int}} = 4\frac{\alpha}{\beta}\text{arccosh}(\frac{d}{2r})$, where α is the fine structure constant and $\beta = \frac{v}{c}$. The resulting χ_{int} is independent of l because the mutual capacitance of the channels is proportional to their length. The interaction strength can be controlled by setting the geometry of the channels and the

electron kinetic energy, $E = m_e c^2 \left(\frac{1}{\sqrt{1-\beta^2}} - 1 \right)$, where m_e is the electron's mass. For instance, for $d = 10r$ and electron kinetic energy of $E = 100$ keV, the interaction strength is $\chi_{\text{int}} = 0.122$, which for $N = 40$ electrons provides more than a factor of 2 improvement in the phase uncertainty, from $\Delta\phi_{\text{SQL}} \approx 0.158$ to $\Delta\phi_W \approx 0.063$. The Coulomb squeezer can be adjusted to larger N values for which the optimal χ_{int} is smaller, e.g., by reducing the distance d between the channels.

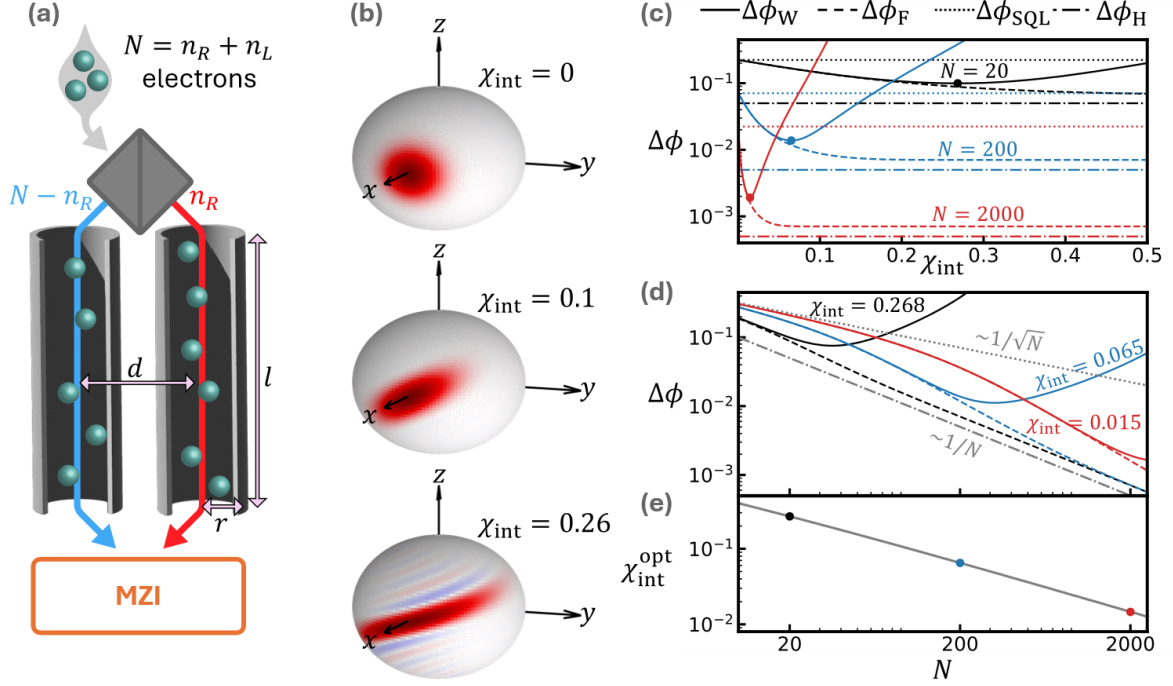


Fig. 2: Interaction-based squeezer. Free-electron analogue of one-axis twisting. (a) **Squeezer schematic:** After the beamsplitter, the electrons are passed through two conductive channels, inducing entanglement through capacitive coupling. (b) **Wigner functions of the resulting squeezed states** correspond to $\chi_{\text{int}} = 0, 0.1, 0.26$ and $N = 20$ electrons. A subsequent rotation (around the x -axis) is necessary to align the squeezed axis properly for improving phase sensitivity. (c) **Phase uncertainty $\Delta\phi$ as a function of χ_{int} ,** comparing: $\Delta\phi_W$ (solid lines) the phase uncertainty of the squeezed interferometer with highlighted points marking minimal values, $\Delta\phi_F$ (dashed lines) the best achievable phase uncertainty, $\Delta\phi_{\text{SQL}}$ (dotted lines) the standard quantum limit, and $\Delta\phi_H$ (dashdotted lines) the Heisenberg limit. Different colors correspond to $N = 20, 200, 2000$ electrons. (d) **Phase uncertainty as a function of N** with different colors correspond to $\chi_{\text{int}} = 0.268, 0.065, 0.015$ shown along $\Delta\phi_{\text{SQL}}$ ($\chi_{\text{int}} = 0$) (dotted lines) and $\Delta\phi_H$ (dashdotted lines). (e) **Optimal interaction strength values χ_{int} that achieve the minimal phase uncertainty $\Delta\phi_W$ as a function of N .** The highlighted points correspond to the minimal phase uncertainties highlighted in (c), for $N = 20, 200, 2000$.

The one-axis twisting operator generated by the Coulomb squeezer produces a state with a minimal spin projection uncertainty along an oblique direction, as shown in Fig. 2b. This tilt can be compensated by rotating the collective state by an extra angle $\delta =$

$\frac{1}{2} \arctan \left(\frac{4 \sin(\chi/2) \cos^{N-2}(\chi/2)}{1 - \cos^{N-2}(\chi)} \right)$ [26,35], which can be implemented by adjusting the coupling coefficient of the input beamsplitter of the MZI.

Performing interferometric measurements on input states prepared via one-axis twisting provides a substantial quantum enhancement that grows with N . The phase uncertainties $\Delta\phi_W$ (Eq. (2)) and $\Delta\phi_F$ (Eq. (3)) as a function of N and χ_{int} are plotted in Fig. 2c and Fig. 2d. For any given N , the phase uncertainty improves with increasing interaction strength χ_{int} up to an optimal squeezing strength $\chi_{\text{int}}^{\text{opt}}$. Fig. 2e shows the optimal squeezing strength as a function of N , calculated by finding the minimum value of $\Delta\phi_W$. At the optimal interaction strength, the spin squeezing parameter scales as $\xi^2 \propto N^{-2/3}$, which corresponds to the best achievable squeezing for one-axis twisting [42,35]. Thus, the capacitive Coulomb squeezer can provide phase measurement accuracy well beyond the SQL, although not quite reaching the Heisenberg limit.

Interestingly, conventional interferometric measurements with one-axis-twisted states do not reach the Heisenberg limit because such measurements do not fully utilize the information contained in the output states, as can be assessed using Fisher information. The lower bound of the phase uncertainty for the squeezed state scales as $\Delta\phi_F \propto N^{-1}$ (Fig. 2d), suggesting the potential to reach the Heisenberg limit. Indeed, at $\chi_{\text{int}} = \pi$ the interaction-based squeezer generates a GHZ state [47], which gives the minimal phase uncertainty of $\Delta\phi_F = N^{-1}$ [48]. In this case, the Heisenberg limited accuracy can be realized by performing a parity measurement on the output state of the interferometer [49]. Experimental realization of this scheme, however, is more difficult than spin-squeezed interferometry, as it is more sensitive to electron loss and dephasing in the sample and puts more stringent requirements on electron detection accuracy.

3.2 Measurement-based squeezer

In a measurement-based squeezer, measuring the number of electrons in one (or both) of the interferometer arms reduces the uncertainty of the number of electrons passing through that arm, thereby creating a squeezed state in \hat{S}_z (Fig. 3). For the two electron paths to remain coherent after measurement, the measuring device must be insensitive to any properties of the electron's state, such as energy and arrival time, which may distinguish between individual

electrons. In other words, the measurement must determine the total number of electrons in each arm of the interferometer without measuring the which-path information of individual electrons. This method, illustrated in Fig. 3a, is inspired by the use of quantum non-demolition measurements, which have been explored for enhanced atomic interferometry [50,15,51,42].

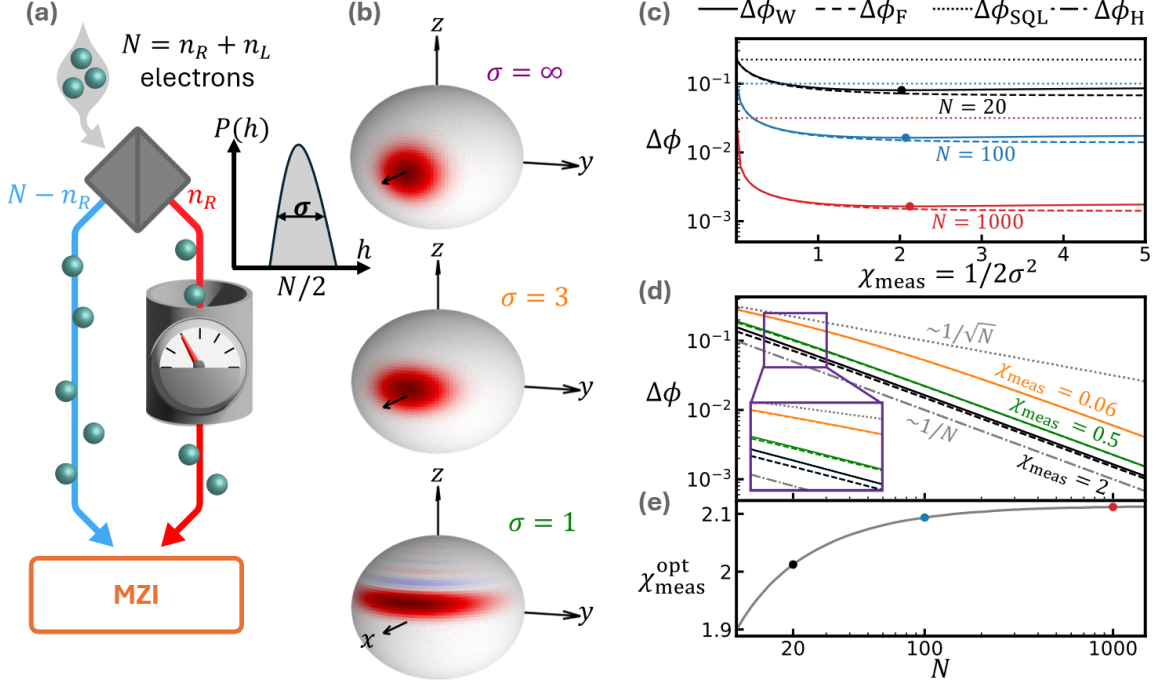


Fig. 3: Measurement-based squeezer. Free-electron analogue of quantum non-demolition measurement. (a) **Squeezer schematic:** After the beamsplitter, the right path passes through the measurement device, which counts the number of electrons. (b) **Wigner functions of the resulting squeezed states** correspond to $\sigma = \infty, 3, 1$, ($\chi_{\text{meas}} = 0, 0.06, 0.5$) and $N = 20$ electrons, with measurement result $h = 7$. (c) **Phase uncertainty $\Delta\phi$ as a function of χ_{meas}** , comparing: $\Delta\phi_W$ (solid lines) the phase uncertainty of the squeezed interferometer, with highlighted points marking minimal values, $\Delta\phi_F$ (dashed lines) the best achievable phase uncertainty, $\Delta\phi_{\text{SQL}}$ (dotted lines) the standard quantum limit, and $\Delta\phi_H$ (dashdotted lines) the Heisenberg limit. Different colors correspond to $N = 20, 100, 1000$ electrons. (d) **Phase uncertainty as a function of N** with different colors correspond to $\chi_{\text{meas}} = 0.06, 0.5, 2$ ($\sigma = 3, 1, 0.5$) shown along $\Delta\phi_{\text{SQL}}$ ($\chi_{\text{meas}} = 0$) (dotted lines) and $\Delta\phi_H$ (dashdotted lines). (e) **Optimal interaction strength values χ_{meas} that achieve the minimal phase uncertainty $\Delta\phi_W$ as a function of N .** The highlighted points correspond to the minimal phase uncertainties highlighted in (c), for $N = 20, 100, 1000$.

The quantum non-demolition measurements can be described in terms of Kraus operators [52]. We analyze here the case where the measurement noise is normally distributed around zero with variance σ^2 . In the case of, for example, measuring the number of electrons in the right arm \hat{n}_R , the Kraus operator is:

$$\hat{K}_{\text{meas}}(h) = \frac{1}{\text{norm}} e^{-\frac{\chi_{\text{meas}}}{2}(\hat{n}_R - h)^2} = \frac{1}{\text{norm}} e^{-\frac{\chi_{\text{meas}}}{2}\left(\frac{N}{2} - \hat{s}_z - h\right)^2}, \quad (5)$$

where h is the measurement result and $\chi_{\text{meas}} = \frac{1}{2\sigma^2}$. The measurement will produce different results on every run, due to both the quantum uncertainty of \hat{n}_R and the measurement error σ . For any h , the Kraus operator action on the electron state $|\psi_0\rangle$ produces a state $\hat{K}_{\text{meas}}(h)|\psi_0\rangle$, squeezed in the z direction as well as offset from the equator of the Bloch sphere by $\frac{N}{2} - h$ (Fig. 3b). The sub-shot-noise limited phase estimate is then obtained by subtracting h from the final measurement of \hat{S}_z .

Performing interferometric measurements on input states prepared via quantum non-demolition measurements provides a substantial quantum enhancement that grows with N . To quantify it, for each measurement result h we calculate the spin-squeezing parameter $\xi^2(h)$ and the quantum Fisher information $F(h)$. We then average over all possible measurement result h with the probabilities $p(h) = |\hat{K}_{\text{meas}}(h)|\psi_0\rangle|^2$ to obtain the phase uncertainties: $\Delta\phi_W = \frac{1}{\sqrt{N}} \sqrt{\int_{-\infty}^{+\infty} p(h) \xi^2(h) dh}$ and $\Delta\phi_F = \int_{-\infty}^{+\infty} \frac{p(h)}{\sqrt{F(h)}} dh$. We find analytically that $\Delta\phi_F = 1/\sqrt{N + \frac{N^2 - N}{2}(1 - e^{-\chi_{\text{meas}}})}$ (SM Section 2.4), which for small enough σ , follows Heisenberg scaling.

The phase uncertainties $\Delta\phi_W$ (calculated numerically) and $\Delta\phi_F$ as a function of N and χ_{meas} are plotted in Fig. 3c and Fig. 3d. For any given N , the phase uncertainty improves with increasing χ_{meas} up to an optimal squeezing strength $\chi_{\text{meas}}^{\text{opt}}$. Fig. 3e shows the optimal squeezing strength as a function of N , calculated by finding the minimum value of $\Delta\phi_W$.

Remarkably, Fig. 3e shows that the optimal squeezing strength is in the vicinity of $\chi_{\text{meas}}^{\text{opt}} = 2$, corresponding to $\sigma = \frac{1}{2}$, for any number of electrons N . Intuitively, this can be understood as follows. To provide a metrological improvement, σ must be smaller than the quantum projection noise: $\sigma < \sqrt{N/2}$. In the limit of precise electron-number measurement where $\sigma \ll \frac{1}{2}$, each measurement projects the electrons into a Dicke state, which cannot be readily used for interferometry. In contrast, in the weak squeezing regime where $1/2 \ll \sigma < \sqrt{N/2}$, phase uncertainty decreases with decreasing σ . Thus, useful squeezing can be achieved in the intermediate range where $1/2 \lesssim \sigma \ll \sqrt{N}$, with the optimal squeezing strength then being $\sigma \approx 1/2$.

As an example, measurement-based free-electron spin squeezing can be implemented using electron interaction with a microwave cavity [53,54]. Following the first beamsplitter shown in Fig. 3a, one of the interferometer arms is passed through a microwave cavity designed so that only one of its modes couples to the electrons, e.g., via phase-matching [55,56]. The electron beam must be temporally bunched to synchronize the electrons arrival time with the phase of the cavity mode [57]. The electrons passing through the cavity collectively create a photonic coherent state with amplitude $\alpha = n_R \sqrt{\chi_{\text{meas}}/2}$. Here, the interaction strength χ_{meas} equals the parameter $2|g_Q^2|$ that is often used to characterize the coupling between the electrons and the cavity [58–63]. The squeezing is then created by a measurement of the amplitude α [64]. The cavity is assumed to be cold enough that its thermal excitation will not affect the measurement accuracy. To maintain coherence of the electron state, the energy uncertainty due to bunching must be large enough that the energy loss via radiation into the cavity mode does not reveal the which-path information.

Strong interaction between the cavity and the electrons is needed to achieve strong spin squeezing. This condition can be relaxed by initializing the cavity with a photonic squeezed vacuum state (see SM Section 2.1 for detailed results and derivation).

4. Discussion and outlook

4.1 Squeezed interferometry in electron microscopy

Spin-squeezing electron interferometry can provide a substantial improvement of the phase measurement accuracy at the electron doses suitable for cryo-EM. We note that even a moderate improvement in the SNR of an imaging system can have a profound effect on the field, as illustrated by the transition from scintillator-based cameras to direct electron detectors, which increased the SNR roughly twofold, playing a major role in bringing about the “resolution revolution” in cryo-EM.

Electron beam-induced damage constrains the dose to about 20 electrons per square angstrom [1], or approximately 1.5x higher at liquid Helium temperatures [65]. Consequently, suitable batch sizes range from about $N \approx 20$ for a typical high-resolution cryo-EM pixel size of 1 Å, to $N \approx 2000$ for a resolution of 10 Å, suitable for cryo-EM of larger structures. Note that on average only $\frac{1}{2} N$ electrons pass through the sample at each pixel in this scheme.

For example, at $N = 40$ electrons, an optimal interaction-based squeezer will require $\chi_{\text{int}} \approx 0.177$, providing more than a factor of 2 improvement in the phase uncertainty, from $\Delta\phi_{\text{SQL}} \approx 0.158$ to $\Delta\phi_{\text{W}} \approx 0.055$. However, even with suboptimal squeezing of $\chi_{\text{int}} \approx 0.122$ that can be achieved with capacitors ratio of $d = 10r$, the phase uncertainty also improves by more than a factor of 2 to $\Delta\phi_{\text{W}} \approx 0.063$. For the same electron dose, an optimal measurement-based squeezer will require $\chi_{\text{meas}} \approx 2.06$, providing a factor 4 improvement in phase sensitivity of $\Delta\phi_{\text{W}} \approx 0.04$. As another example, at $N = 2000$, optimal squeezers with $\chi_{\text{int}} \approx 0.015$ and $\chi_{\text{meas}} \approx 2.12$, the phase uncertainty improves by more than an order of magnitude, from $\Delta\phi_{\text{SQL}} \approx 0.023$ to $\Delta\phi_{\text{W}} \approx 0.002$ and $\Delta\phi_{\text{W}} \approx 0.001$, for the interaction-based and measurement-based squeezers, respectively. These results demonstrate that optimal squeezing strength can be achieved with realistic squeezer parameters across the entire resolution range relevant to cryo-EM, establishing spin squeezing as a natural modality of quantum metrology for application in electron microscopy.

4.2 Model limitations

In the initial analysis provided in this paper, we did not consider electron losses to both elastic and inelastic scattering in the sample, and possible losses in the elements of the interferometer. Spin-squeezing is known to be among the most robust quantum-metrology approaches, less sensitive to electron losses than other entanglement-based quantum metrology schemes. The mean free path of electrons in amorphous ice ranges from roughly 300 nm at 300 keV to 200 nm at 100 keV [66]. Consequently, in a typical thin cryo-EM sample of about 30 nm, the share of electrons lost to inelastic scattering is in the range of 0.1 to 0.2. For thicker samples, such as 100-200 nm lamellae used in cryo-ET [67], imaged at 300 keV, that share is in the range of 0.3 to 0.5. While this level of electron loss limits the useful strength of squeezing [16], it still allows for a significant metrological improvement. This relatively robust behavior of spin-squeezed electron states contrasts with more fragile fully entangled states such as GHZ, which loses the phase information with loss of even a single electron in a batch.

4.3 Prospects for experimental realization

In addition to the squeezer devices discussed above, experimental realization of a spin-squeezed electron Mach-Zehnder interferometer requires a coherent, low-loss beamsplitter to

split and recombine the electron waves, and a low-noise electron detector. We now briefly review the state of technology for each of those components.

Electron beamsplitters: Conventionally, electron interference has been observed by electron holography using an electrostatic biprism (a “wavefront splitter” device) and observing electron interference fringes. However, to implement spin squeezing interferometry schemes envisioned here, a true “amplitude splitter” is needed. Interferometry with amplitude-splitting electron beamsplitters have been realized with membrane-based diffraction gratings [68–71,13], although such membranes are inherently lossy due to electron scattering. A theoretical proposal has been made to create a nearly lossless beamsplitter based on a diffraction grating embedded in an electrostatic electron resonator [72]. In parallel, significant research efforts are dedicated to the development of a practically lossless electron beamsplitters based on electron confinement in guiding channels by either RF ponderomotive potential [73,74] or auto-ponderomotive potential created by electrostatic fields of alternating polarity [75,76]. These on-going efforts make it probable that a nearly lossless beamsplitter will be created over the next few years.

Electron detectors: Electron detectors have been developing rapidly in recent years and have already reached a sufficient signal-to-noise ratio to enable squeezed interferometry. Several types of detectors (monolithic CMOS direct electron detectors, hybrid pixel sensors) have been developed that operate in the electron-counting mode, detecting individual electron arrival events. Quantum efficiency of such detectors can be as high as 0.94 [77] or even 0.98 [78]. Thus, already existing electron detectors technology can be used to read out the number of electrons in each port of the interferometer with deeply sub-shot-noise limited accuracy.

Measurement-based free-electron spin squeezing can be implemented using an optical structure rather than the microwave cavity considered above. An optical implementation can rely on efficient cathodoluminescence [79–81] whereby the electron becomes entangled with the photon it emits [82,83]. Sufficient energy uncertainty to maintain path interference after the interaction with the cavity can be achieved using short (e.g., attosecond [84–86]) electron pulse trains.

The concept of free-electron spin-squeezing can thus contribute to the wider field of free-electron quantum optics [87,88], which so far mostly focused on electron-light interactions [89–91,64,92,93], rather than on electron phase sensitivity. The approach suggested here for

measurement-based electron spin squeezing can help create various forms of entangled free-electron and photonic states that can be harnessed in other areas of quantum science [60,61,94,64,92,82,83].

We analyzed electron spin squeezing in a scanning interferometer configuration that surveys samples pixel by pixel. Signal acquisition can be parallelized with a multi-channel squeezer of the same conceptual design. Alternatively, a wide-field spin-squeezed imaging can potentially be implemented using a squeezer device capable of multi-mode entanglement, based, e.g., on collective emission of light by electrons interacting with an extended object, such as a membrane or a sheet of cathodoluminescent material.

4.4 Summary

In summary, we have shown that spin squeezing can be used to overcome the seemingly fundamental limitation of the SNR in transmission electron microscopy posed by shot noise. The necessary spin-squeezed electron states can be generated in a variety of ways with either existing or emerging technologies, providing a robust and practical pathway toward quantum-enhanced electron microscopy. By contributing to the development of cryo-EM and cryo-ET, spin-squeezing electron microscopy may become one of the few applications of quantum metrology with significance extending beyond the field of quantum physics.

Acknowledgments

This research is funded by the European Union- ERC COG, QinPINEM, Project Number 101125662. This research is also funded (in part) by the Gordon and Betty Moore Foundation, through Grant GBMF11473. O.S. acknowledges financial support from the Gordon and Betty Moore Foundation, the Israel Science Foundation (ISF), and the Center for New Scientists at the Weizmann Institute of Science. E.S. acknowledges financial support from the Israel Science Foundation (ISF), the Directorate for Defense Research and Development (DDR&D), the Minerva Foundation with funding from the Federal German Ministry for Education and Research, and the Center for New Scientists at the Weizmann Institute of Science. S.E.-H. acknowledges financial support from the Ariane de Rothschild Women Doctoral Program. R.R. acknowledges financial support from the ADAMS Fellowship Program of the Israel Academy of Sciences and Humanities.

References

- [1] R. M. Glaeser and R. J. Hall, Reaching the Information Limit in Cryo-EM of Biological Macromolecules: Experimental Aspects, *Biophysical Journal* **100**, 2331 (2011).
- [2] Y. Cheng, Single-particle cryo-EM—How did it get here and where will it go, *Science* **361**, 876 (2018).
- [3] A.-C. Milazzo et al., Active pixel sensor array as a detector for electron microscopy, *Ultramicroscopy* **104**, 152 (2005).
- [4] G. McMullan, S. Chen, R. Henderson, and A. R. Faruqi, Detective quantum efficiency of electron area detectors in electron microscopy, *Ultramicroscopy* **109**, 1126 (2009).
- [5] R. Danev, B. Buijsse, M. Khoshouei, J. M. Plitzko, and W. Baumeister, Volta potential phase plate for in-focus phase contrast transmission electron microscopy, *Proceedings of the National Academy of Sciences* **111**, 15635 (2014).
- [6] O. Schwartz, J. J. Axelrod, S. L. Campbell, C. Turnbaugh, R. M. Glaeser, and H. Müller, Laser phase plate for transmission electron microscopy, *Nat Methods* **16**, 1016 (2019).
- [7] V. Giovannetti, S. Lloyd, and L. Maccone, Quantum-Enhanced Measurements: Beating the Standard Quantum Limit, *Science* **306**, 1330 (2004).
- [8] W. P. Putnam and M. F. Yanik, Noninvasive electron microscopy with interaction-free quantum measurements, *Phys. Rev. A* **80**, 040902 (2009).
- [9] H. Okamoto, Possible use of a Cooper-pair box for low-dose electron microscopy, *Phys. Rev. A* **85**, 043810 (2012).
- [10] P. Kruit et al., Designs for a quantum electron microscope, *Ultramicroscopy* **164**, 31 (2016).
- [11] T. Juffmann, S. A. Koppell, B. B. Klopfer, C. Ophus, R. M. Glaeser, and M. A. Kasevich, Multi-pass transmission electron microscopy, *Sci Rep* **7**, 1699 (2017).
- [12] S. A. Koppell, M. Mankos, A. J. Bowman, Y. Israel, T. Juffmann, B. B. Klopfer, and M. A. Kasevich, Design for a 10 keV multi-pass transmission electron microscope, *Ultramicroscopy* **207**, 112834 (2019).
- [13] A. E. Turner, C. W. Johnson, P. Kruit, and B. J. McMorran, Interaction-Free Measurement with Electrons, *Phys. Rev. Lett.* **127**, 110401 (2021).
- [14] B. Yurke, Interferometry with correlated fermions, *Physica B+C* **151**, 286 (1988).
- [15] M. Kitagawa and M. Ueda, Nonlinear-interferometric generation of number-phase-correlated fermion states, *Phys. Rev. Lett.* **67**, 1852 (1991).
- [16] S. A. Koppell, Y. Israel, A. J. Bowman, B. B. Klopfer, and M. A. Kasevich, Transmission electron microscopy at the quantum limit, *Applied Physics Letters* **120**, 190502 (2022).
- [17] H. Okamoto and Y. Nagatani, Entanglement-assisted electron microscopy based on a flux qubit, *Applied Physics Letters* **104**, 062604 (2014).
- [18] H. Okamoto, R. Firouzmandi, R. Miyamura, V. Sazgari, S. Okumura, S. Uchita, and I. I. Kaya, TEM at millikelvin temperatures: Observing and utilizing superconducting qubits, *Micron* **161**, 103330 (2022).
- [19] J. Aasi et al., Enhanced sensitivity of the LIGO gravitational wave detector by using squeezed states of light, *Nature Photon* **7**, 613 (2013).
- [20] R. Schnabel, Squeezed states of light and their applications in laser interferometers, *Physics Reports* **684**, 1 (2017).
- [21] M. Tse et al., Quantum-Enhanced Advanced LIGO Detectors in the Era of Gravitational-Wave Astronomy, *Phys. Rev. Lett.* **123**, 231107 (2019).
- [22] Y. Michael, L. Bello, M. Rosenbluh, and A. Pe’er, Squeezing-enhanced Raman spectroscopy, *Npj Quantum Inf* **5**, 1 (2019).
- [23] C. A. Casacio, L. S. Madsen, A. Terrasson, M. Waleed, K. Barnscheidt, B. Hage, M. A. Taylor, and W. P. Bowen, Quantum-enhanced nonlinear microscopy, *Nature* **594**, 201 (2021).

- [24] Z. Xu, K. Oguchi, Y. Taguchi, S. Takahashi, Y. Sano, T. Mizuguchi, K. Katoh, and Y. Ozeki, Quantum-enhanced stimulated Raman scattering microscopy in a high-power regime, *Opt. Lett.*, **OL 47**, 5829 (2022).
- [25] K. M. Backes et al., A quantum enhanced search for dark matter axions, *Nature* **590**, 238 (2021).
- [26] M. Kitagawa and M. Ueda, Squeezed spin states, *Phys. Rev. A* **47**, 5138 (1993).
- [27] V. Meyer, M. A. Rowe, D. Kielpinski, C. A. Sackett, W. M. Itano, C. Monroe, and D. J. Wineland, Experimental Demonstration of Entanglement-Enhanced Rotation Angle Estimation Using Trapped Ions, *Phys. Rev. Lett.* **86**, 5870 (2001).
- [28] J. Appel, P. J. Windpassinger, D. Oblak, U. B. Hoff, N. Kjærgaard, and E. S. Polzik, Mesoscopic atomic entanglement for precision measurements beyond the standard quantum limit, *Proceedings of the National Academy of Sciences* **106**, 10960 (2009).
- [29] I. D. Leroux, M. H. Schleier-Smith, and V. Vuletić, Implementation of Cavity Squeezing of a Collective Atomic Spin, *Phys. Rev. Lett.* **104**, 073602 (2010).
- [30] M. H. Schleier-Smith, I. D. Leroux, and V. Vuletić, States of an Ensemble of Two-Level Atoms with Reduced Quantum Uncertainty, *Phys. Rev. Lett.* **104**, 073604 (2010).
- [31] M. H. Schleier-Smith, I. D. Leroux, and V. Vuletić, Squeezing the collective spin of a dilute atomic ensemble by cavity feedback, *Phys. Rev. A* **81**, 021804 (2010).
- [32] C. Gross, T. Zibold, E. Nicklas, J. Estève, and M. K. Oberthaler, Nonlinear atom interferometer surpasses classical precision limit, *Nature* **464**, 1165 (2010).
- [33] E. G. Dalla Torre, J. Otterbach, E. Demler, V. Vuletic, and M. D. Lukin, Dissipative Preparation of Spin Squeezed Atomic Ensembles in a Steady State, *Phys. Rev. Lett.* **110**, 120402 (2013).
- [34] O. Hosten, N. J. Engelsen, R. Krishnakumar, and M. A. Kasevich, Measurement noise 100 times lower than the quantum-projection limit using entangled atoms, *Nature* **529**, 505 (2016).
- [35] L. Pezzè, A. Smerzi, M. K. Oberthaler, R. Schmied, and P. Treutlein, Quantum metrology with nonclassical states of atomic ensembles, *Rev. Mod. Phys.* **90**, 035005 (2018).
- [36] Th. Leuthner, H. Lichte, and K.-H. Herrmann, STEM-holography using the electron biprism, *Physica Status Solidi (a)* **116**, 113 (1989).
- [37] C. W. Johnson, A. E. Turner, and B. J. McMorran, Scanning two-grating free electron Mach-Zehnder interferometer, *Phys. Rev. Research* **3**, 043009 (2021).
- [38] R. H. Dicke, Coherence in Spontaneous Radiation Processes, *Phys. Rev.* **93**, 99 (1954).
- [39] J. P. Dowling, G. S. Agarwal, and W. P. Schleich, Wigner distribution of a general angular-momentum state: Applications to a collection of two-level atoms, *Phys. Rev. A* **49**, 4101 (1994).
- [40] D. J. Wineland, J. J. Bollinger, W. M. Itano, F. L. Moore, and D. J. Heinzen, Spin squeezing and reduced quantum noise in spectroscopy, *Phys. Rev. A* **46**, R6797 (1992).
- [41] D. J. Wineland, J. J. Bollinger, W. M. Itano, and D. J. Heinzen, Squeezed atomic states and projection noise in spectroscopy, *Phys. Rev. A* **50**, 67 (1994).
- [42] J. Ma, X. Wang, C. P. Sun, and F. Nori, Quantum spin squeezing, *Physics Reports* **509**, 89 (2011).
- [43] S. L. Braunstein and C. M. Caves, Statistical distance and the geometry of quantum states, *Phys. Rev. Lett.* **72**, 3439 (1994).
- [44] M. G. A. Paris, Quantum estimation for quantum technology, *Int. J. Quantum Inform.* **07**, 125 (2009).
- [45] S. Uhlemann, Thermal Magnetic Field Noise Limits Resolution in Transmission Electron Microscopy, *Phys. Rev. Lett.* **111**, (2013).
- [46] J. D. Jackson, *Classical Electrodynamics* (John Wiley & Sons, 1998).
- [47] B. Yurke and D. Stoler, Generating quantum mechanical superpositions of macroscopically distinguishable states via amplitude dispersion, *Phys. Rev. Lett.* **57**, 13 (1986).
- [48] H. Lee, P. Kok, and J. P. Dowling, A Quantum Rosetta Stone for Interferometry, *Journal of Modern Optics* **49**, 2325 (2002).
- [49] J. J. Bollinger, W. M. Itano, D. J. Wineland, and D. J. Heinzen, Optimal frequency measurements with maximally correlated states, *Phys. Rev. A* **54**, R4649 (1996).

- [50] M. Kitagawa, N. Imoto, and Y. Yamamoto, Realization of number-phase minimum-uncertainty states and number states by quantum nondemolition measurement, *Phys. Rev. A* **35**, 5270 (1987).
- [51] A. Kuzmich, L. Mandel, and N. P. Bigelow, Generation of Spin Squeezing via Continuous Quantum Nondemolition Measurement, *Phys. Rev. Lett.* **85**, 1594 (2000).
- [52] K. Kraus, General state changes in quantum theory, *Annals of Physics* **64**, 311 (1971).
- [53] W. Verhoeven, J. F. M. van Rens, E. R. Kieft, P. H. A. Mutsaers, and O. J. Luiten, High quality ultrafast transmission electron microscopy using resonant microwave cavities, *Ultramicroscopy* **188**, 85 (2018).
- [54] Q. Yan, R. Ruimy, A. Niedermayr, and I. Kaminer, *Single-Particle–Single-Photon Coupling Using a Circuital Metamaterial Cavity*, in *CLEO 2023 (2023), Paper FF3D.1* (Optica Publishing Group, 2023), p. FF3D.1.
- [55] R. Dahan et al., Resonant phase-matching between a light wave and a free-electron wavefunction, *Nat. Phys.* **16**, 11 (2020).
- [56] G. Huang, N. J. Engelsen, O. Kfir, C. Ropers, and T. J. Kippenberg, Electron-Photon Quantum State Heralding Using Photonic Integrated Circuits, *PRX Quantum* **4**, 020351 (2023).
- [57] L. Schächter, *Beam-Wave Interaction in Periodic and Quasi-Periodic Structures* (Springer Science & Business Media, 2011).
- [58] O. Kfir, Entanglements of Electrons and Cavity Photons in the Strong-Coupling Regime, *Phys. Rev. Lett.* **123**, 103602 (2019).
- [59] V. D. Giulio, M. Kociak, and F. J. G. de Abajo, Probing quantum optical excitations with fast electrons, *Optica*, *OPTICA* **6**, 1524 (2019).
- [60] R. Dahan, G. Baranes, A. Gorlach, R. Ruimy, N. Rivera, and I. Kaminer, Creation of Optical Cat and GKP States Using Shaped Free Electrons, *Phys. Rev. X* **13**, 031001 (2023).
- [61] G. Baranes, S. Even-Haim, R. Ruimy, A. Gorlach, R. Dahan, A. A. Diringer, S. Hacoheh-Gourgy, and I. Kaminer, Free-electron interactions with photonic GKP states: Universal control and quantum error correction, *Phys. Rev. Research* **5**, 043271 (2023).
- [62] Z. Xie, Z. Chen, H. Li, Q. Yan, H. Chen, X. Lin, I. Kaminer, O. D. Miller, and Y. Yang, Maximal Quantum Interaction between Free Electrons and Photons, *Phys. Rev. Lett.* **134**, 043803 (2025).
- [63] Z. Zhao, Upper Bound for the Quantum Coupling between Free Electrons and Photons, *Phys. Rev. Lett.* **134**, 043804 (2025).
- [64] R. Ruimy, O. Tziperman, A. Gorlach, K. Mølmer, and I. Kaminer, Many-body entanglement via ‘which-path’ information, *Npj Quantum Inf* **10**, 1 (2024).
- [65] J. L. Dickerson, K. Naydenova, M. J. Peet, H. Wilson, B. Nandy, G. McMullan, R. Morrison, and C. J. Russo, Reducing the effects of radiation damage in cryo-EM using liquid helium temperatures, *Proceedings of the National Academy of Sciences* **122**, e2421538122 (2025).
- [66] M. J. Peet, R. Henderson, and C. J. Russo, The energy dependence of contrast and damage in electron cryomicroscopy of biological molecules, *Ultramicroscopy* **203**, 125 (2019).
- [67] L. N. Young and E. Villa, Bringing Structure to Cell Biology with Cryo-Electron Tomography, *Annual Review of Biophysics* **52**, 573 (2023).
- [68] A. Caprez, R. Bach, S. McGregor, and H. Batelaan, A wide-angle electron grating bi-prism beam splitter, *J. Phys. B: At. Mol. Opt. Phys.* **42**, 165503 (2009).
- [69] F. S. Yasin, K. Harada, D. Shindo, H. Shinada, B. J. McMorran, and T. Tanigaki, A tunable path-separated electron interferometer with an amplitude-dividing grating beamsplitter, *Applied Physics Letters* **113**, 233102 (2018).
- [70] T. R. Harvey et al., Interpretable and Efficient Interferometric Contrast in Scanning Transmission Electron Microscopy with a Diffraction-Grating Beam Splitter, *Phys. Rev. Appl.* **10**, 061001 (2018).
- [71] C. W. Johnson, A. E. Turner, and B. J. McMorran, Scanning two-grating free electron Mach-Zehnder interferometer, *Phys. Rev. Res.* **3**, 043009 (2021).
- [72] Y. Yang, C.-S. Kim, R. G. Hobbs, P. Kruit, and K. K. Berggren, Efficient two-port electron beam splitter via a quantum interaction-free measurement, *Phys. Rev. A* **98**, 043621 (2018).

- [73] J. Hammer, S. Thomas, P. Weber, and P. Hommelhoff, Microwave Chip-Based Beam Splitter for Low-Energy Guided Electrons, *Phys. Rev. Lett.* **114**, 254801 (2015).
- [74] R. Zimmermann, P. Weber, M. Seidling, and P. Hommelhoff, Beam splitting of low-energy guided electrons with a two-sided microwave chip, *Applied Physics Letters* **115**, 104103 (2019).
- [75] R. Zimmermann, M. Seidling, and P. Hommelhoff, Charged particle guiding and beam splitting with auto-ponderomotive potentials on a chip, *Nat Commun* **12**, 1 (2021).
- [76] M. Seidling, R. Zimmermann, and P. Hommelhoff, Chip-based electrostatic beam splitting of guided kiloelectron volt electrons, *Applied Physics Letters* **118**, 034101 (2021).
- [77] M. W. Tate et al., High Dynamic Range Pixel Array Detector for Scanning Transmission Electron Microscopy, *Microscopy and Microanalysis* **22**, 237 (2016).
- [78] G. McMullan et al., Structure determination by cryoEM at 100 keV, *Proceedings of the National Academy of Sciences* **120**, e2312905120 (2023).
- [79] J.-W. Henke et al., Integrated photonics enables continuous-beam electron phase modulation, *Nature* **600**, 653 (2021).
- [80] N. Varkentina et al., Cathodoluminescence excitation spectroscopy: Nanoscale imaging of excitation pathways, *Science Advances* **8**, eabq4947 (2022).
- [81] Y. Adiv et al., Observation of 2D Cherenkov Radiation, *Phys. Rev. X* **13**, 011002 (2023).
- [82] J.-W. Henke, H. Jeng, M. Sivi, and C. Ropers, *Observation of Quantum Entanglement between Free Electrons and Photons*, arXiv:2504.13047.
- [83] A. Preimesberger, S. Bogdanov, I. C. Bicket, P. Rembold, and P. Haslinger, *Experimental Verification of Electron-Photon Entanglement*, arXiv:2504.13163.
- [84] K. E. Priebe, C. Rathje, S. V. Yalunin, T. Hohage, A. Feist, S. Schäfer, and C. Ropers, Attosecond electron pulse trains and quantum state reconstruction in ultrafast transmission electron microscopy, *Nature Photon* **11**, 12 (2017).
- [85] Y. Morimoto and P. Baum, Diffraction and microscopy with attosecond electron pulse trains, *Nature Phys* **14**, 252 (2018).
- [86] M. Kozák, N. Schönenberger, and P. Hommelhoff, Ponderomotive Generation and Detection of Attosecond Free-Electron Pulse Trains, *Phys. Rev. Lett.* **120**, 103203 (2018).
- [87] R. Ruimy, A. Karnieli, and I. Kaminer, Free-electron quantum optics, *Nat. Phys.* **21**, 193 (2025).
- [88] F. J. G. de Abajo et al., *Roadmap for Quantum Nanophotonics with Free Electrons*, arXiv:2503.14678.
- [89] E. Rotunno et al., One-Dimensional “Ghost Imaging” in Electron Microscopy of Inelastically Scattered Electrons, *ACS Photonics* **10**, 1708 (2023).
- [90] S. Kumar, J. Lim, N. Rivera, W. Wong, Y. S. Ang, L. K. Ang, and L. J. Wong, Strongly correlated multielectron bunches from interaction with quantum light, *Sci. Adv.* **10**, eadm9563 (2024).
- [91] E. Kazakevich, H. Aharon, and O. Kfir, Spatial electron-photon entanglement, *Phys. Rev. Res.* **6**, 043033 (2024).
- [92] J.-W. Henke, H. Jeng, and C. Ropers, Probing electron-photon entanglement using a quantum eraser, *Phys. Rev. A* **111**, 012610 (2025).
- [93] C. I. Velasco and F. J. G. de Abajo, *Quantum Sensing and Metrology with Free Electrons*, arXiv:2505.06124.
- [94] A. Karnieli, S. Tsesses, R. Yu, N. Rivera, A. Arie, I. Kaminer, and S. Fan, Universal and Ultrafast Quantum Computation Based on Free-Electron-Polariton Blockade, *PRX Quantum* **5**, 010339 (2024).